THE EUROPEAN
PHYSICAL JOURNAL C

Measuring the Hubble constant with cosmic chronometers: a machine learning approach

Carlos Bengaly[1,a] , **Maria Aldinez Dantas**[2,b], **Luciano Casarini**[3,c], **Jailson Alcaniz**[1,d]

[1] Observatório Nacional, Rio de Janeiro, RJ 20921-400, Brazil
[2] Departamento de Física, Universidade do Estado do Rio Grande do Norte, Mossoró, RN 59610-210, Brazil
[3] Departamento de Física, Universidade Federal de Sergipe, São Cristóvão, SE 49000, Brazil

Abstract Local measurements of the Hubble constant (H_0) based on Cepheids e Type Ia supernova differ by $\approx 5\sigma$ from the estimated value of H_0 from Planck CMB observations under ΛCDM assumptions. In order to better understand this H_0 tension, the comparison of different methods of analysis will be fundamental to interpret the data sets provided by the next generation of surveys. In this paper, we deploy machine learning algorithms to measure the H_0 through a regression analysis on synthetic data of the expansion rate assuming different values of redshift and different levels of uncertainty. We compare the performance of different regression algorithms as Extra-Trees, Artificial Neural Network, Gradient Boosting, Support Vector Machines, and we find that the Support Vector Machine exhibits the best performance in terms of bias-variance tradeoff in most cases, showing itself a competitive cross-check to non-supervised regression methods such as Gaussian Processes.

1 Introduction

The standard model of Cosmology consists of a flat, homogeneous and isotropic universe whose energy content is dominated by a cosmological constant (Λ) and cold dark matter (ΛCDM) [1,2]. Such a model provides the best description of cosmological observations such as temperature fluctuations of the Cosmic Microwave Background (CMB) [3], luminosity distances to Type Ia Supernovae (SNe) [4], large-scale

clustering of galaxies (LSS), and weak gravitational lensing (WL) [5–8]. Despite its tremendous success, this model presents theoretical caveats, such as the value of the vacuum energy density [9,10], in addition to observational challenges e.g. the $\simeq 5\sigma$ Hubble constant tension between CMB and SNe observations [11–13], as well as milder tensions between matter density perturbation estimates from CMB and LSS, and slightly enhanced CMB lensing amplitude than predicted by the ΛCDM model. These conflicting measurements may hint at physics beyond the standard cosmology.

Given the necessity to probe the Universe at larger and deeper scales, cosmological surveys like Javalambre-Physics of the Accelerated Universe Astrophysical Survey (J-PAS) [14,15], Dark Energy Spectroscopic Instrument (DESI) [16], Euclid [17], Square Kilometer Array (SKA) [18] and the Large Synoptic Survey Telescope (LSST) [19] were proposed and developed. They will improve the constraints we currently have on the parameters of the ΛCDM model, and probe departures from it with unprecedented sensitivity. In order to extract the most of cosmological information from the tantalising amount of data to come, the deployment of machine learning (ML) algorithms on Physics and Astronomy [20,21] is becoming crucial to accelerate data processing and improve statistical inference. Some recent applications of ML on Cosmology focuses on reconstructing the late-time cosmic expansion history to test fundamental hypothesis of the standard model and constrain its parameters [22–35], cosmological model discrimination with LSS and WL [36–46], predicting structure formation [47–57], probing the era of reionisation [58–64], photometric redshift estimation [65–72], besides the classification of astrophysical sources [73–76] and transient objects [77–80]. These analyses reveal that ML algorithms are able to recover the underlying cosmology from data and simulations with greater precision than traditionally used techniques e.g. 2-point correlation function and

[a] e-mail: carlosbengaly@on.br (corresponding author)

[b] e-mail: aldinezdantas@uern.br

[c] e-mail: lcasarini@academico.ufs.br

[d] e-mail: alcaniz@on.br

power spectrum, in addition to Markov Chain Monte Carlo (MCMC) methods.

In this paper we discuss the ability to measure the Hubble Constant H_0 from cosmic chronometers measurements $(H(z))$ using different ML algorithms. We first produce $H(z)$ synthetic data-sets with different number of data points and measurement uncertainties, in order to perform a benchmark test of the H_0 constraints for each algorithms given the quality of the input data. Rather than performing a numerical reconstruction across the redshift range probed by the data, and then fitting H_0, we carry out an extrapolation of the reconstructed $H(z)$ values down to $z = 0$. We also compare their performance with other non-parametric reconstruction methods, such as the popularly adopted Gaussian Processes (GAP) [81]. Our goal is to verify whether they can provide a competitive cross-check with the GAP.

The paper is structured as follows: Sect. 2 is dedicated to the cosmological framework and the simulations produced for our analysis. Section 3 explains how this analysis is performed, along with the metrics adopted for algorithm performance evaluation. Section 4 presents our results; finally our main conclusions and final remarks are presented in Sect. 5.

2 Simulations

2.1 Prescription

In order to compare how different predicting algorithm perform with different quality of data, we produce sets of $H(z)$ simulated data sets and adopt the following prescription:

(i) We assume as fiducial cosmology the flat ΛCDM model given by Planck 2018 (TT, TE, EE+lowE+lensing; hereafter P18) [3]:

$$H_0^{\text{fid}} = 67.36 \pm 0.54 \, \text{km} \, \text{s}^{-1} \, \text{Mpc}^{-1} \tag{1}$$
$$\Omega_m^{\text{fid}} = 0.3166 \pm 0.0084 \tag{2}$$
$$\Omega_\Lambda^{\text{fid}} = 1 - \Omega_m, \tag{3}$$

so that the Hubble parameter follows the Friedmann equation for the fiducial ΛCDM model

$$\left[\frac{H^{\text{fid}}(z)}{H_0^{\text{fid}}} \right]^2 = \Omega_m^{\text{fid}}(1+z)^3 + \Omega_\Lambda^{\text{fid}}. \tag{4}$$

(ii) We compute the values of $H(z)$ considering the N_z data points following a redshift distribution $p(z)$ such as [27]

$$p(z; \, k, \theta) = z^{k-1} \frac{e^{-z/\theta}}{\theta^k \Gamma(k)} \,, \tag{5}$$

where we fix θ and k to their respective best fits to the real cosmic chronometers data, as in [27], i.e., $\theta_{\text{bf}} = 0.647$ and $k = 1.048$.

(iii) In order to understand how our knowledge of $H(z)$ along the redshift space affects the performance of the statistical learning, we provide different sets of $H(z)$ assuming different numbers of points $N_z = 20, 30, 50$ and 80, and assuming different relative uncertainties values, i.e., $\sigma_H/H = 0.008, 0.01, 0.03, 0.05, 0.08$. This variation of N_z and $\sigma_H(z)$ allows to evaluate what level of accuracy of measurements of $H(z)$ is necessary in order to obtain a specific precision on the prediction of H_0.

(iv) We also produce $H(z)$ simulations based on the current cosmic chronometer data, which consists of $N_z = 31$ measurements presented in 1 – see also Table I in [27].

Such a prescription provides a benchmark to test the performance of the ML algorithms deployed.

2.2 Uncertainty estimation

Although these algorithms are able to provide measurements of H_0 at a given redshift, they do not provide their uncertainties. We develop a Monte Carlo-bootstrap (MC-bootstrap) method for this purpose, described as follows

- Rather than creating a single simulation centered on the fiducial model for each data-set (item (i) of Sect. 2), we produce $H(z)$ measurements at a given redshift following a normal distribution centred around its fiducial value according to $\mathcal{N}(H^{\text{fid}}(z), \sigma_H/H)$. $H^{\text{fid}}(z)$ represents the $H(z)$ value given by the fiducial Cosmology, whereas σ_H consists on its uncertainty as described in the item (iii) of Sect. 2.
- As for the "real data" simulations, described in item (iv) of Sect. 2, we replace the ith $H(z)$ measurement presented in the second column of Table 1 by a value drawn from a normal distribution centered on the fiducial model, i.e, $\mathcal{N}(H^{\text{fid}}(z_i), \sigma_{H;i})$, where z_i represents the redshift of each data point and $\sigma_{H;i}$ its corresponding uncertainty – first and third columns in Table 1, respectively.
- We repeat this procedure 100 times for each data-set of N_z data-points with σ_H/H uncertainties as described in the item (iii) and (iv) of Sect. 2.
- The 100 MC realisations produced for each case are provided as inputs for each ML algorithms described in Sect. 3.1.
- We report the average and standard deviation of these 100 values as the H_0 measurement and uncertainty, respectively, for each N_z and σ_H/H case. Same applies for the "real data" simulations.

Table 1 31 CC $H(z)$ measurements obtained from the differential age method used in our analysis

z	$H(z)$ (km s^{-1} Mpc^{-1})	References
0.09	69 ± 12	[82]
0.17	83 ± 8	
0.27	77 ± 14	
0.4	95 ± 17	
0.9	117 ± 23	[83]
1.3	168 ± 17	
1.43	177 ± 18	
1.53	140 ± 14	
1.75	202 ± 40	
0.48	97 ± 62	[84]
0.88	90 ± 40	
0.1791	75 ± 4	
0.1993	75 ± 5	
0.3519	83 ± 14	
0.5929	104 ± 13	[85]
0.6797	92 ± 8	
0.7812	105 ± 12	
0.8754	125 ± 17	
1.037	154 ± 20	
0.07	69 ± 19.6	
0.12	68.6 ± 26.2	[86]
0.2	72.9 ± 29.6	
0.28	88.8 ± 36.6	
1.363	160 ± 33.6	[87]
1.965	186.5 ± 50.4	
0.3802	83 ± 13.5	
0.4004	77 ± 10.2	
0.4247	87.1 ± 11.2	[88]
0.44497	92.8 ± 12.9	
0.4783	80.9 ± 9	
0.47	89 ± 49.6	[89]

3 Analysis

3.1 Methods

Our regression analysis are carried out on all simulated and "real" data-sets with several ML algorithms available in the `scikit-learn` package[1] [90]. Firstly we divide our input sample into training and testing data-sets as

```
z_train,z_test,hz_train,hz_test =
train_test_split(z,hz,test_size=0.25,
random_state=42)
```

so that our testing sub-set contains 25% of the original sample size. Then we deploy different ML algorithms on the training test, looking for the "best combination" of hyperparameters with the help of *GridSearchCV*.[2] This function of `scikit-learn`, given a ML method, performs the learning with all the combination of hyperparameters and shows the performance of every combination – or each one of them – during the cross-validation (CV) procedure .[3] Such a procedure is performed for the sake of avoiding overfitting on the test set. We chose CV = 3 in our analysis, given the limited number of $H(z)$ data-points.

The ML methods deployed in our analysis are given as follows:

- **Extra-Trees (EXT)**: An ensemble of randomised decision trees (extra-trees). The goal of the algorithm is to create a model that predicts the value of a target variable by learning simple decision rules inferred from the data features. A tree can be seen as a piecewise constant approximation[4] [91]. We evaluate the algorithm hyperpameter values that best fit the input simulations through a grid search. Hence, our grid search over the EXT hyperpameters are given by:

```
gcv = GridSearchCV(ExtraTreesRegressor
(min_samples_split=2,
random_state=42),
param_grid={
'n_estimators': np.arange(1,100,2),
'max_depth': np.arange(1,10,2),
cv=3, refit=True)
```

- **Artificial Neural Network (ANN)**: A Multi-layered Perceptron algorithm that trains using backpropagation with no activation function in the output layer[5] [92]. The ANN hyperparameter grid search consists of:

```
gcv = GridSearchCV(MLPRegressor
({activation='relu'},
solver='lbfgs',
learning_rate='adaptive',
max_iter=200,
random_state=42),
param_grid={
'hidden_layer_sizes': np.arange(10,250,10),
},
cv=3, refit=True)
```

---

[1] https://scikit-learn.org/stable/.

[2] https://scikit-learn.org/stable/modules/generated/sklearn.model_selection.GridSearchCV.html.

[3] https://scikit-learn.org/stable/modules/cross_validation.html.

[4] https://scikit-learn.org/stable/modules/tree.html.

[5] https://scikit-learn.org/stable/modules/neural_networks_supervised.html.

- **Gradient Boosting Regression (GBR)**: This estimator builds an additive model in a forward stage-wise fashion; it allows for the optimisation of arbitrary differentiable loss functions. In each stage a regression tree is fit on the negative gradient of the given loss function [6] [93]. The grid search over the GBR hyperparameters corresponds to:

```
gcv = GridSearchCV(
GradientBoostingRegressor(random_state=42),
param_grid={
'n_estimators': np.arange(1,200,5),
},
cv=3, refit=True)
```

- **Support Vector Machines (SVM)**: A linear model that creates a line or hyperplane to separate data into different classes [94,95]. Originally developed for classification problems, it was also extended for regression, as in the goal of this work.[7] The hyperparameter grid search of the SVM method reads

```
gcv = GridSearchCV(SVR(kernel='poly',
C=100,
gamma='auto', epsilon=.1,
coef0=1),
param_grid={
'degree': np.arange(1, 10),},
cv=3, refit=True)
```

Note that we adopted the default evaluation metric for each ML algorithm as defined by the `scikit-learn` package. So the EXT method uses the squared error metric to define the quality of the tree split – likewise for the GBR and ANN loss functions - whereas the SVM method assumes $\epsilon = 0.1$, so that samples whose prediction is at least ϵ away from their true target are penalised.[8]

In order to evaluate the performance of these methods, we report the results of the training and test score as

```
print(gcv.best_estimator_.predict([[0.]]),
gcv.score(z_train,hz_train),
gcv.score(z_test,hz_test))
```

Moreover, we deploy the well-known Gaussian Processes regression (GAP) algorithm on the same simulated data-sets using the GAPP package [81]. We compare the results obtained with the ML algorithms just described with GAP

since the latter has been widely used in the literature for similar purposes for about a decade. Two GAP kernels are assumed in our analysis, namely the Squared Exponential (SqExp) and Matérn(5/2) (Mat52). We justify these choices on the basis that the SqExp kernel exhibits greater differentiability than the Mat52, which may result in a larger degree of smoothing on the data reconstruction – hence, smaller reconstruction uncertainties – that may or may not fully represent the underlying data.

3.2 Robustness of results

We define the bias (b) as the average displacement of the predicted Hubble Constant (H_0^{pred}), obtained from the MC-bootstrap method, from the fiducial value, i.e., $\Delta H_0 = H_0^{\mathrm{pred}} - H_0^{\mathrm{fid}}$, and the Mean Squared Error (MSE) as the average squared displacement:

$$\mathrm{b} = \langle \Delta H_0 \rangle, \quad \mathrm{MSE} = \langle \Delta H_0^2 \rangle. \tag{6}$$

Using the definition of variance, we estimate the bias-variance tradeoff of our analysis

$$\mathrm{BVT} = \langle \Delta H_0^2 \rangle - \langle \Delta H_0 \rangle^2 = \mathrm{MSE} - \mathrm{b}^2, \tag{7}$$

therefore we can evaluate the performance of these algorithms for each simulated data-set specification.

4 Results

We show our H_0 measurements for each algorithm in Fig. 1. The top panels present the results obtained from the EXT (left) and ANN (right) algorithms, whereas the middle panels display the GBR (left) and SVM (right) results, and the bottom ones show the GAP predictions for the Mat52 and SqExp kernels in the left and right plots, respectively. Each data point at these plots represents the predicted H_0 values (H_0^{pred}) according to the prescription described in Sect. 2.1 for each simulated data-set specifications, i.e., different σ_H/H results against the N_z values. The light blue horizontal line corresponds to the fiducial H_0. We can see that GBR and EXT are able to correctly predict the fiducial H_0 for higher N_z and lower σ_H/H values, but not otherwise – especially for low values of N_z, where these algorithms predict a larger H_0 value. This indicates a bias in the results, despite the cross-validation procedure adopted. We also find that ANN and SVM are able to recover the fiducial H_0, even for lower quality sets of simulations. However, its predictions present larger variances as σ_H/H increases.

These results show that GBR and EXT are more sensitive to N_z concerning bias, whereas ANN is more sensitive to σ_H/H with respect to its variance. On the other hand, SVM exhibits the best bias-variance tradeoff among all algorithms,
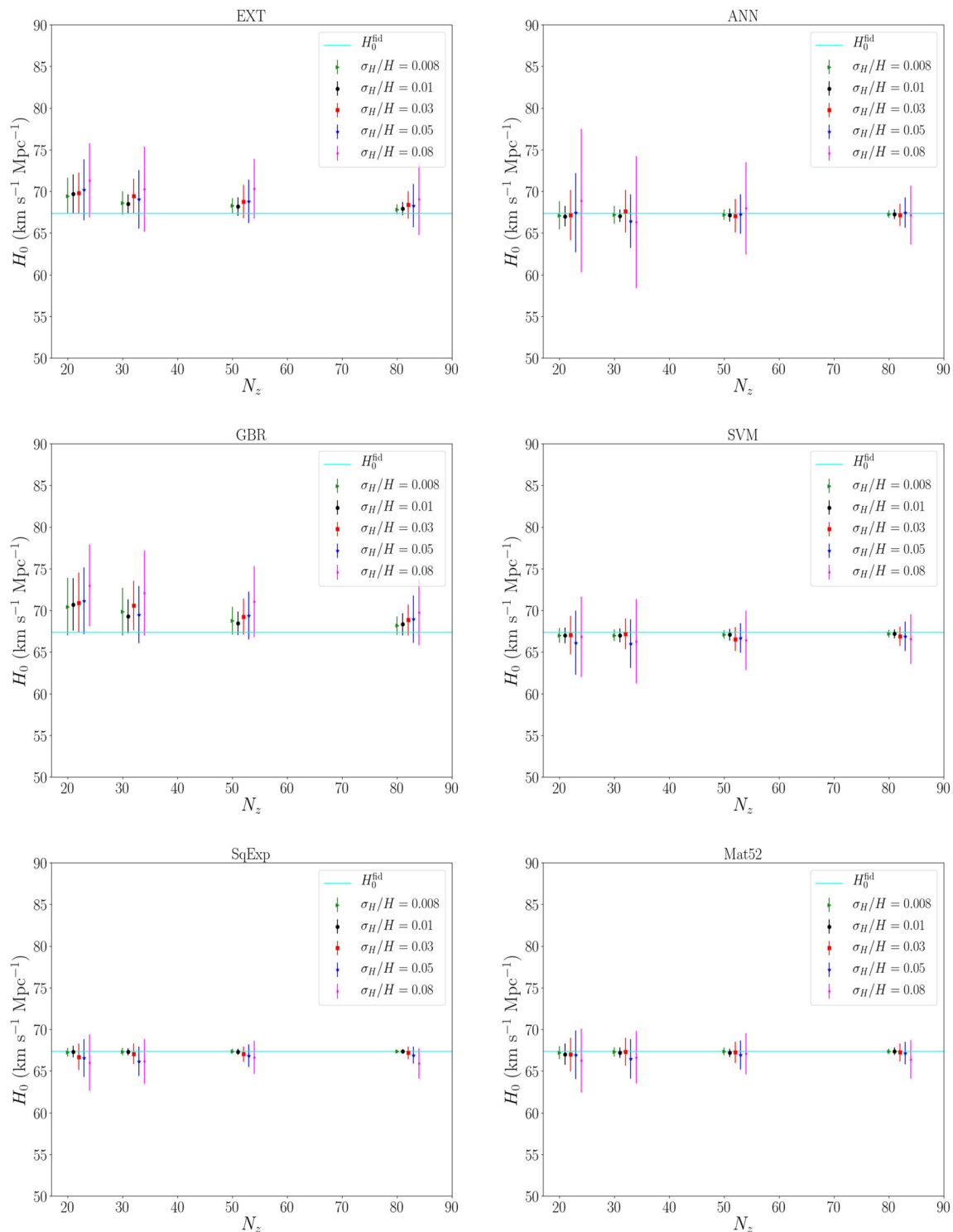

Fig. 1 H_0 measurements from the algorithm EXT (top left), ANN (top right), GBR (center left), SVM (center right), SqExp (lower left) and Mat52 (lower right), plotted against the number of simulated $H(z)$ measurements. Each data point represents different σ_H/H values, whereas the light blue horizontal lines denote the fiducial H_0 value

as shown in Fig. 2, along with Tables 2, 3, 4, 5 and 6, presented in Appendix B. We obtain that SVM is able to recover the fiducial H_0 without significant losses in bias and variance

as the simulation quality decreases. Such a result may happen due to a few reasons: For example, due to the non-guaranteed convergence of neural networks. By an appropriate choice of
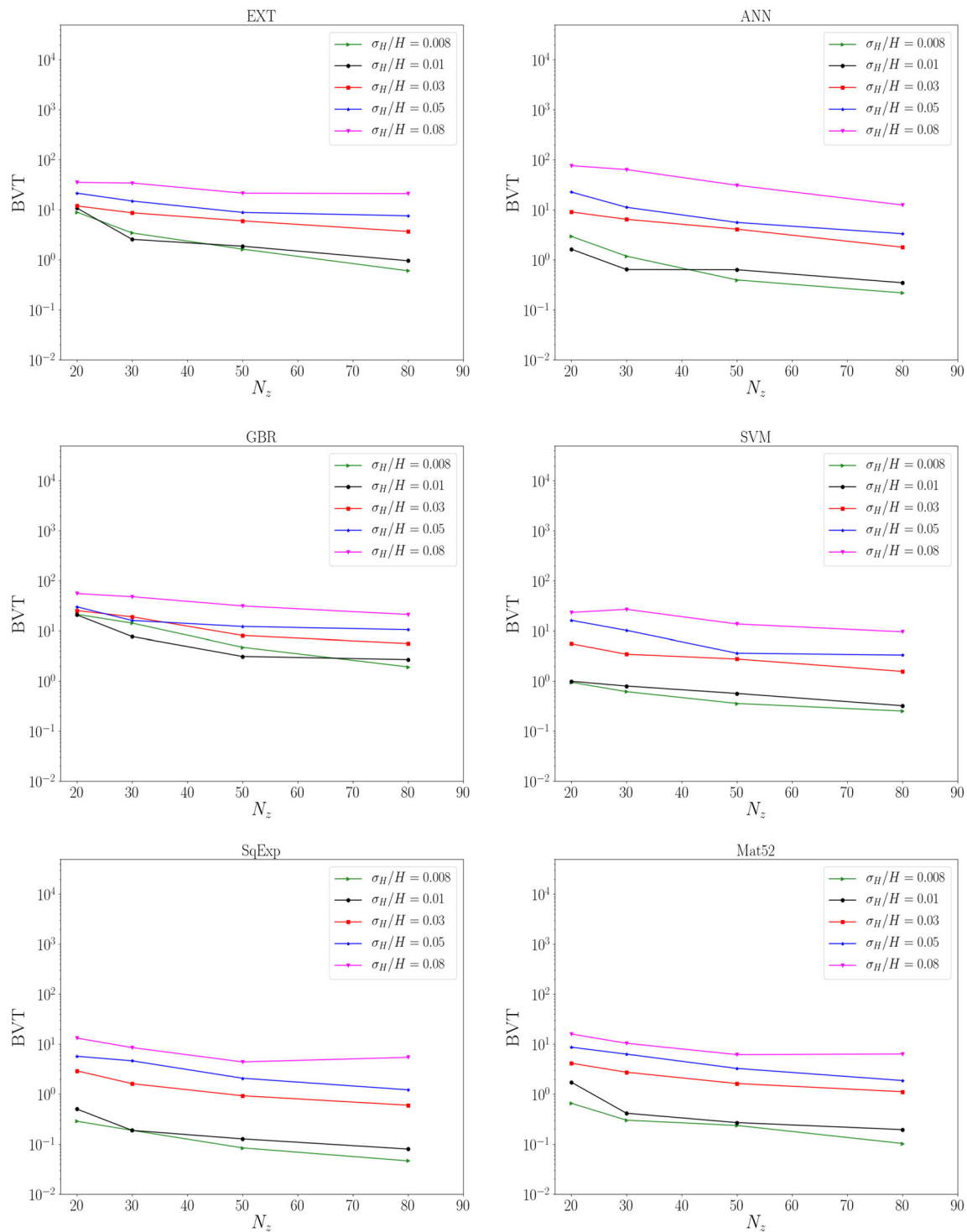
Fig. 2 Same as Fig. 1, but for the BVT. Each data point corresponds to different σ_H/H values

hyperparameters, ANN can approach a target function until a satisfactory result is reached; however, SVMs are theoretically grounded in their capacity to converge to the solution for a problem. Note that we adopted a polynomial kernel for SVM, and a nonlinear activation function for ANN, namely

"relu", in order to make a fair comparison between them. As for the EXT case, such an algorithm is known to be prone to overfitting and to outliers, which can explain the larger bias with lower variance. A similar problem applies for the GBR case as well. Not to mention that both demand a longer
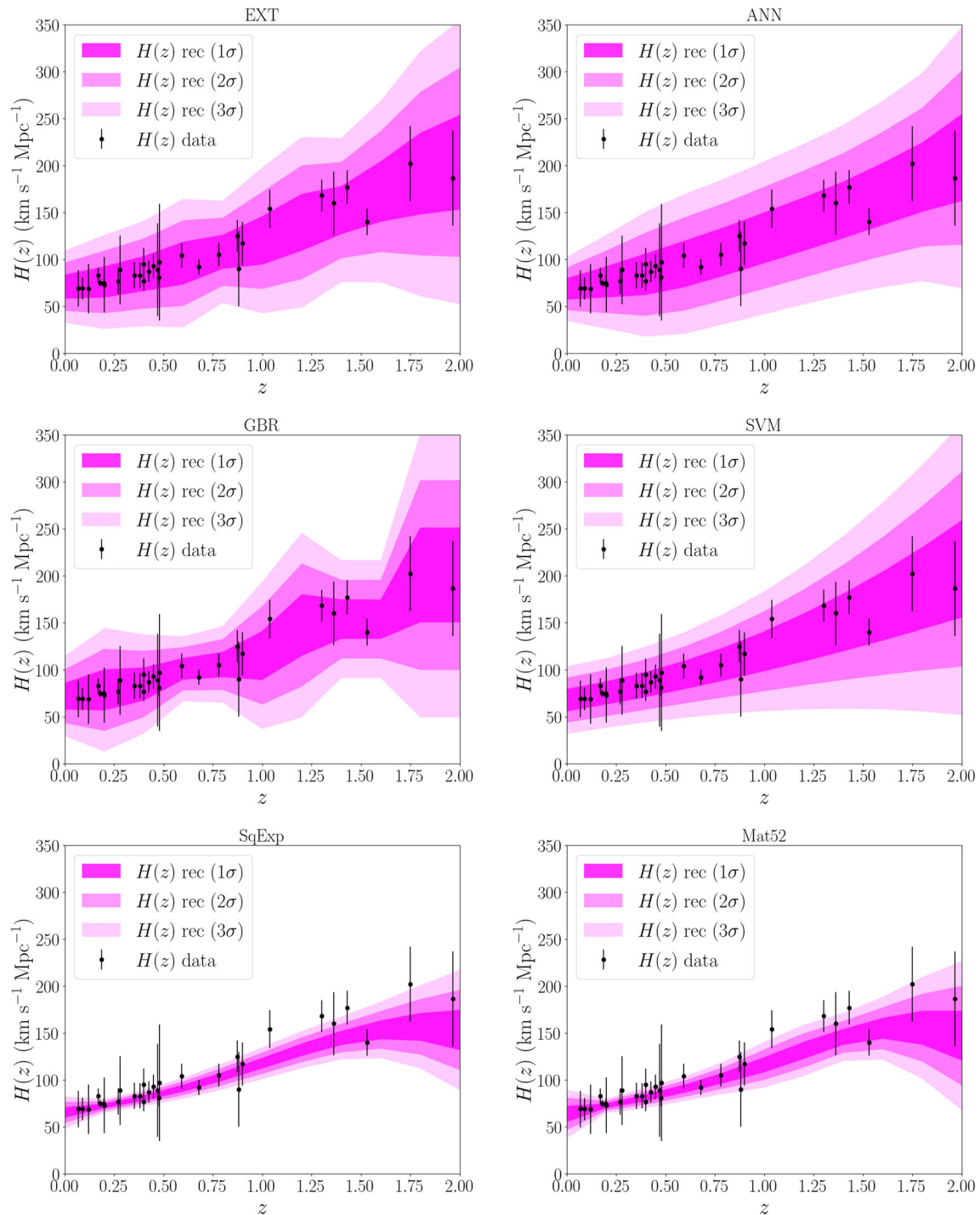
Fig. 3 The reconstructed $H(z)$ values obtained from EXT (top left), ANN (top right), GBR (center left), SVM (center right), SqExp (lower left) and Mat52 (lower right). Different shades of magenta represent different confidence level for the reconstructions, ranging from 1 (darker shade) to 3σ (lighter shade)

training time than ANN and SVM, which translates into a longer computational time to obtain the H_0 measurements and uncertainties in our case.

Regarding the comparison with the results obtained with GAP using the Squared Exponential (SqExp) and Matérn(5/2) (Mat52) kernels, we find good agreement between the SVM and GAP measurement of H_0, in spite of a

slightly larger BVT for the former. But note that GAP can also be prone to overfitting, as the data points with smaller uncertainties have a greater impact to determine the function that best represents the distance between data points to perform its numerical reconstruction – especially when assuming the SqExp kernel, which presents greater differentiability than the Mat52 case. Therefore, we show that SVM can be used as a cross-check method for GAP regression, which has been widely used in the literature..

Moreover, we show the $H(z)$ reconstructions obtained from the simulations mimicking the real data configuration in Fig. 3, at a 1, 2 and 3σ confidence level, alongside the actual $H(z)$ measurements. We can clearly see a "step-wise" behaviour on the EXT and GBR reconstructions, contrarily to other algorithms. This illustrates the bias problems they face, as commented before. Once again, the GAP results exhibit the smallest uncertainties among all, but this may also happen due to possible overfitting, as commented before. This is exemplified by the dip on the high-z end of the reconstruction. Nevertheless, the Hubble Constant measured by all algorithms are in agreement with each other, as depicted in Table 7, where EXT and GBR again exhibit a tendency towards larger H_0 values – and hence larger BVT – while ANN and SVM present less biased results, as in the previous cases. Interestingly, we find that ANN performed slightly better than SVM this time around, yielding a slightly lower BVT. Note also that our results are in good agreement with the predicted H_0 in [27], who used ANN as well in their analysis,[9] but we could obtain a slightly lower uncertainty in our predictions – roughly 17% uncertainty versus 23% in their case.

We also checked whether the test sample size affects the H_0 predictions and their bias-variance tradeoff. We find that its default choice, i.e., a split between 75 and 25% between training and test sample, respectively, provides the best results for all algorithms compared to a 90–10% and 60–40% split, for instance. The EXT and GBR algorithms perform similarly for 10% and 25%, but their predictions become significantly worse for the 40% case. This is an expected result, since both algorithms require large training sets to carry out such predictions. On the other hand, ANN and SVM perform significantly worse for split choices other than the default one. Finally, we verified the results for different cross-validations values, such as CV = 2, 4, 8, finding consistent values with those obtained with the standard choice CV = 3.

5 Conclusions

Machine learning has been gaining formidable importance in present times. Given the state-of-art of modern computation and processing facilities, the application of machine learning algorithms in physical sciences not only became popular, but essential in the process of handling huge data-sets and performing model prediction - specially in light of forthcoming redshift surveys.

Our work focused on a comparison of different machine learning algorithms for the sake of measuring the Hubble Constant from cosmic chronometers measurements. We used four different algorithms in our analysis, which are based on decision trees, artificial neural networks, support vector machine and gradient boosting, as available in the `scikit-learn` python package. We applied them on simulated $H(z)$ data-sets assuming different specifications, and assuming a flat ΛCDM model consistent with Planck 2018 best fit, in order to measure H_0 through an extrapolation procedure.

Our uncertainties are estimated using a Monte Carlo-bootstrap method on the simulations, after properly splitting them into training and test sets, and performed a grid search over their hyperparameter space during the cross-validation procedure. In addition, we created a performance ranking between these methods via the bias-variance tradeoff, and compared them with other established methods in the literature, e.g. Gaussian Processes as in the GAPP code.

We obtained that the algorithms based on decision trees and gradient boosting present the lowest performance among all, as they provide low variance with a large bias in the reconstructed H_0. Instead, the artificial neural networks and support vector machine are able to correctly recover the fiducial H_0 value, where the latter method exhibits the lowest variance among them. We also found that the support vector machine algorithm presents compatible benchmark metrics with the Gaussian Processes one. This result shows that such method can be successfully used as a cross-check method between different non-parametric reconstruction techniques, which will be of great importance in the advent of next-generation cosmological surveys [14–19], as they are expected to provide $H(z)$ measurements with a few percent precision.

---

[9] The authors reported $H_0 = 67.33 \pm 15.74$ km s^{-1} Mpc^{-1}.

Appendix A: Algorithm performance results

See Tables 2, 3, 4, 5, 6 and 7.

Table 2 Respectively: H_0 measurements (in units of $\mathrm{km s^{-1}\ Mpc^{-1}}$), as well as the BVT values obtained for all N_z and ML algorithms assuming $\sigma_H/H = 0.008$. We also show the results obtained using the GAP method at the bottom of the table

alg	N_z	$H_0 \pm \sigma_{H_0}$	BVT
EXT	20	69.443 ± 2.151	8.966
	30	68.593 ± 1.385	3.438
	50	68.288 ± 0.877	1.632
	80	67.844 ± 0.607	0.601
ANN	20	67.111 ± 1.695	2.936
	30	67.179 ± 1.071	1.180
	50	67.198 ± 0.606	0.395
	80	67.262 ± 0.456	0.217
GBR	20	70.441 ± 3.456	21.438
	30	69.837 ± 2.857	14.296
	50	68.747 ± 1.673	4.723
	80	68.170 ± 1.124	1.920
SVM	20	66.973 ± 0.892	0.946
	30	67.004 ± 0.698	0.614
	50	67.090 ± 0.533	0.357
	80	67.181 ± 0.468	0.251
SqExp	20	67.261 ± 0.527	0.287
	30	67.286 ± 0.428	0.188
	50	67.374 ± 0.290	0.084
	80	67.343 ± 0.215	0.046
Mat52	20	67.189 ± 0.792	0.657
	30	67.312 ± 0.545	0.302
	50	67.351 ± 0.486	0.236
	80	67.363 ± 0.321	0.103

Table 3 Same as Table 2, but assuming $\sigma_H/H = 0.01$

alg	N_z	$H_0 \pm \sigma_{H_0}$	BVT
EXT	20	69.678 ± 2.334	10.818
	30	68.491 ± 1.132	2.560
	50	68.157 ± 1.111	1.869
	80	67.928 ± 0.796	0.955
ANN	20	66.999 ± 1.224	1.629
	30	67.064 ± 0.743	0.639
	50	67.148 ± 0.767	0.637
	80	67.255 ± 0.579	0.346
GBR	20	70.682 ± 3.140	20.894
	30	69.276 ± 2.009	7.706
	50	68.431 ± 1.398	3.103
	80	68.325 ± 1.324	2.685
SVM	20	67.005 ± 0.930	0.990
	30	66.990 ± 0.812	0.796
	50	67.074 ± 0.696	0.566
	80	67.179 ± 0.537	0.321
SqExp	20	67.321 ± 0.708	0.503
	30	67.286 ± 0.428	0.188
	50	67.300 ± 0.352	0.127
	80	67.354 ± 0.282	0.080
Mat52	20	67.011 ± 1.270	1.735
	30	67.213 ± 0.627	0.415
	50	67.183 ± 0.488	0.270
	80	67.352 ± 0.442	0.195

Table 4 Same as Table 2, but assuming $\sigma_H/H = 0.03$

alg	N_z	$H_0 \pm \sigma_{H_0}$	BVT
EXT	20	69.787 ± 2.461	11.946
	30	69.407 ± 2.120	8.683
	50	68.762 ± 2.007	5.995
	80	68.377 ± 1.627	3.682
ANN	20	67.140 ± 2.997	9.031
	30	67.610 ± 2.528	6.451
	50	67.059 ± 2.001	4.094
	80	67.169 ± 1.321	1.782
GBR	20	70.906 ± 3.589	25.457
	30	70.566 ± 2.967	19.083
	50	69.236 ± 2.145	8.118
	80	68.843 ± 1.847	5.611
SVM	20	67.016 ± 2.332	5.557
	30	67.152 ± 1.843	3.440
	50	66.538 ± 1.443	2.758
	80	66.879 ± 1.153	1.561

Table 4 continued

alg	N_z	$H_0 \pm \sigma_{H_0}$	BVT
SqExp	20	66.690 ± 1.574	2.925
	30	67.063 ± 1.238	1.622
	50	67.021 ± 0.902	0.929
	80	67.177 ± 0.753	0.601
Mat52	20	66.963 ± 1.998	4.152
	30	67.313 ± 1.657	2.746
	50	67.228 ± 1.270	1.631
	80	67.224 ± 1.049	1.118

Table 5 Same as Table 2, but assuming $\sigma_H/H = 0.05$

alg	N_z	$H_0 \pm \sigma_{H_0}$	BVT
EXT	20	70.189 ± 3.672	21.486
	30	69.039 ± 3.485	14.964
	50	68.805 ± 2.601	8.850
	80	68.281 ± 2.596	7.586
ANN	20	67.445 ± 4.754	22.606
	30	66.417 ± 3.212	11.207
	50	67.272 ± 2.361	5.580
	80	67.460 ± 1.818	3.316
GBR	20	71.122 ± 4.001	30.164
	30	69.474 ± 3.415	16.128
	50	69.374 ± 2.864	12.258
	80	68.938 ± 2.847	10.596
SVM	20	66.111 ± 3.831	16.238
	30	65.993 ± 2.894	10.242
	50	66.680 ± 1.772	3.602
	80	66.881 ± 1.756	3.311
SqExp	20	66.553 ± 2.252	5.722
	30	66.153 ± 1.784	4.641
	50	66.820 ± 1.338	2.082
	80	66.900 ± 1.005	1.221
Mat52	20	66.920 ± 2.914	8.684
	30	66.442 ± 2.340	6.318
	50	66.918 ± 1.753	3.269
	80	67.141 ± 1.350	1.872

Table 6 Same as Table 2, but assuming $\sigma_H/H = 0.08$

alg	N_z	$H_0 \pm \sigma_{H_0}$	BVT
EXT	20	71.322 ± 4.424	35.271
	30	70.248 ± 5.092	34.274
	50	70.305 ± 3.586	21.535
	80	69.040 ± 4.267	21.028
ANN	20	68.874 ± 8.605	76.333
	30	66.293 ± 7.910	63.698
	50	67.952 ± 5.531	30.943
	80	67.143 ± 3.521	12.447
GBR	20	72.979 ± 4.907	55.656
	30	72.081 ± 5.080	48.096
	50	71.026 ± 4.250	31.501
	80	69.742 ± 3.948	21.261
SVM	20	66.813 ± 4.799	23.333
	30	66.271 ± 5.076	26.949
	50	66.395 ± 3.578	13.731
	80	66.563 ± 2.987	9.557
SqExp	20	66.014 ± 3.378	13.224
	30	66.130 ± 2.652	8.544
	50	66.611 ± 1.963	4.413
	80	65.910 ± 1.829	5.448
Mat52	20	66.234 ± 3.832	15.955
	30	66.644 ± 3.147	10.418
	50	67.085 ± 2.471	6.183
	80	66.369 ± 2.316	6.344

Table 7 Same as Table 2, but assuming the real data configuration, i.e., $N_z = 31$ and the same $\sigma_{H(z)}$ of the real $H(z)$ measurements

alg	$H_0 \pm \sigma_{H_0}$	BVT
EXT	70.829 ± 12.839	176.881
ANN	68.412 ± 11.389	130.821
GBR	71.766 ± 14.255	222.620
SVM	67.601 ± 11.982	143.634
SqExp	66.890 ± 6.065	37.005
Mat52	66.355 ± 9.568	92.556

References

1. A.G. Riess et al., [Supernova Search Team], Observational evidence from supernovae for an accelerating universe and a cosmological constant. Astron. J. **116**, 1009–1038 (1998). arXiv:astro-ph/9805201
2. S. Perlmutter et al., [Supernova Cosmology Project], Measurements of Ω and Λ from 42 high redshift supernovae. Astrophys. J. **517**, 565–586 (1999). arXiv:astro-ph/9812133
3. N. Aghanim, et al., [Planck Collaboration], Planck 2018 results. VI. Cosmological parameters. Astron. Astrophys. **641**, A6 (2020). (Erratum: Astron. Astrophys. 652 (2021), C4) arXiv:1807.06209
4. D.M. Scolnic, et al., The complete light-curve sample of spectroscopically confirmed SNe Ia from Pan-STARRS1 and cosmological constraints from the combined pantheon sample. Astrophys. J. **859**(2), 101 (2018). arXiv:1710.00845
5. S. Alam, et al. [eBOSS], The Completed SDSS-IV extended Baryon oscillation spectroscopic survey: cosmological implications from two decades of spectroscopic surveys at the apache point observatory. Phys. Rev. D **103**(8), 083533 (2021). arXiv:2007.08991
6. C. Heymans et al., KiDS-1000 cosmology: multi-probe weak gravitational lensing and spectroscopic galaxy clustering constraints. Astron. Astrophys. **646**, A140 (2021). arXiv:2007.15632

7. T.M.C. Abbott, et al., [DES], Dark energy survey year 3 results: cosmological constraints from galaxy clustering and weak lensing. Phys. Rev. D **105**(2), 023520 (2022). arXiv:2105.13549

8. L.F. Secco, et al. [DES], Dark energy survey year 3 results: cosmology from cosmic shear and robustness to modeling uncertainty. Phys. Rev. D **105**(2), 023515 (2022). arXiv:2105.13544

9. S. Weinberg, The cosmological constant problem. Rev. Mod. Phys. **61**, 1–23 (1989)

10. T. Padmanabhan, Cosmological constant: the weight of the vacuum. Phys. Rep. **380**, 235–320 (2003). arXiv:hep-th/0212290

11. E. Di Valentino, O. Mena, S. Pan, L. Visinelli, W. Yang, A. Melchiorri, D.F. Mota, A.G. Riess, J. Silk, In the realm of the Hubble tension—a review of solutions. Class. Quantum Gravity **38**(15), 153001 (2021). arXiv:2103.01183

12. P. Shah, P. Lemos, O. Lahav, A buyer's guide to the Hubble constant. Astron. Astrophys. Rev. **29**(1), 9 (2021). arXiv:2109.01161

13. A.G. Riess, W. Yuan, L.M. Macri, D. Scolnic, D. Brout, S. Casertano, D.O. Jones, Y. Murakami, L. Breuval, T.G. Brink, et al., A comprehensive measurement of the local value of the hubble constant with 1 km/s/Mpc uncertainty from the hubble space telescope and the SH0ES Team. arXiv:2112.04510

14. N. Benitez, et al., [J-PAS], J-PAS: The Javalambre-physics of the accelerated universe astrophysical survey. arXiv:1403.5237

15. S. Bonoli, et al., The miniJPAS survey: a preview of the Universe in 56 colours. Astron. Astrophys. **653**, A31 (2021). arXiv:2007.01910

16. A. Aghamousa, et al., [DESI Collaboration], The DESI experiment part I: science,targeting, and survey design. arXiv:1611.00036

17. L. Amendola et al., Cosmology and fundamental physics with the Euclid satellite. Living Rev. Relativ. **21**, 2 (2018). arXiv:1606.00180

18. D.J. Bacon et al., [SKA Collaboration], Cosmology with phase 1 of the square kilometre array: red book 2018: technical specifications and performance forecasts. Publ. Astron. Soc. Austral. **37**, e007 (2020). arXiv:1811.02743

19. D. Alonso, et al., [LSST Dark Energy Science], The LSST Dark Energy Science Collaboration (DESC) Science Requirements Document. arXiv:1809.01669

20. G. Carleo et al., Machine learning and the physical sciences. Rev. Mod. Phys. **91**(4), 045002 (2019). arXiv:1903.10563

21. M. Ntampaka, et al., The role of machine learning in the next decade of cosmology. arXiv:1902.10159

22. S.Y. Li, Y.L. Li, T.J. Zhang, Model comparison of dark energy models using deep network. Res. Astron. Astrophys. **19**, 137 (2019). arXiv:1907.00568

23. T. Liu, S. Cao, J. Zhang, S. Geng, Y. Liu, X. Ji, Z.H. Zhu, Implications from simulated strong gravitational lensing systems: constraining cosmological parameters using Gaussian Processes. Astrophys. J. **886**, 94 (2019). arXiv:1910.02592

24. Y. Wu, S. Cao, J. Zhang, T. Liu, Y. Liu, S. Geng, Y. Lian, Exploring the "$L-\sigma$" relation of HII galaxies and giant extragalactic HII regions acting as standard candles. arXiv:1911.10959

25. R. Arjona, S. Nesseris, What can machine learning tell us about the background expansion of the universe? Phys. Rev. D **101**(12), 123525 (2020). arXiv:1910.01529

26. C. Escamilla-Rivera, M.A.C. Quintero, S. Capozziello, A deep learning approach to cosmological dark energy models. JCAP **03**, 008 (2020). arXiv:1910.02788

27. G.J. Wang, X.J. Ma, S.Y. Li, J.Q. Xia, Reconstructing functions and estimating parameters with artificial neural networks: a test with a hubble parameter and SNe Ia. Astrophys. J. Suppl. **246**(1), 13 (2020). arXiv:1910.03636

28. G.J. Wang, S.Y. Li, J.Q. Xia, ECoPANN: a framework for estimating cosmological parameters using artificial neural networks. Astrophys. J. Suppl. **249**(2), 25 (2020). arXiv:2005.07089

29. Y.C. Wang, Y.B. Xie, T.J. Zhang, H.C. Huang, T. Zhang, K. Liu, Likelihood-free cosmological constraints with artificial neural networks: an application on hubble parameters and SN Ia. Astrophys. J. Suppl. **254**(2), 43 (2021). arXiv:2005.10628

30. T. Liu, S. Cao, S. Zhang, X. Gong, W. Guo, C. Zheng, Revisiting the cosmic distance duality relation with machine learning reconstruction methods: the combination of HII galaxies and ultra-compact radio quasars. Eur. Phys. J. C **81**(10), 903 (2021). arXiv:2110.00927

31. C. García, C. Santa, A.E. Romano, Deep learning reconstruction of the large scale structure of he Universe from luminosity distance observations. Mon. Not. R. Astron. Soc. **518**(2), 2241–2246 (2022). arXiv:2107.05771

32. K. Dialektopoulos, J.L. Said, J. Mifsud, J. Sultana, K.Z. Adami, Neural network reconstruction of late-time cosmology and null tests. JCAP **02**(02), 023 (2022). arXiv:2111.11462

33. P. Mukherjee, J.L. Said, J. Mifsud, Neural network reconstruction of $H'(z)$ and its application in teleparallel gravity. JCAP **12**, 029 (2022). arXiv:2209.01113

34. I. Gómez-Vargas, R.M. Esquivel, R. García-Salcedo, J.A. Vázquez, Neural network reconstructions for the Hubble parameter, growth rate and distance modulus. Eur. Phys. J. C **83**(4), 304 (2023). arXiv:2104.00595

35. L. Tonghua, C. Shuo, M. Shuai, L. Yuting, Z. Chenfa, W. Jieci, What are recent observations telling us in light of improved tests of distance duality relation? Phys. Lett. B **838**, 137687 (2023). arXiv:2301.02997

36. S. Agarwal, F.B. Abdalla, H.A. Feldman, O. Lahav, S.A. Thomas, PkANN-I. Non-linear matter power spectrum interpolation through artificial neural networks. Mon. Not. R. Astron. Soc. **424**, 1409–1418 (2012). arXiv:1203.1695

37. S. Agarwal, F.B. Abdalla, H.A. Feldman, O. Lahav, S.A. Thomas, pkann-II. A non-linear matter power spectrum interpolator developed using artificial neural networks. Mon. Not. R. Astron. Soc. **439**(2), 2102–2121 (2014). arXiv:1312.2101

38. S. Ravanbakhsh, J. Oliva, S. Fromenteau, L.C. Price, S. Ho, J. Schneider, B. Poczos, Estimating cosmological parameters from the dark matter distribution. arXiv:1711.02033

39. J. Merten, C. Giocoli, M. Baldi, M. Meneghetti, A. Peel, F. Lalande, J.L. Starck, V. Pettorino, On the dissection of degenerate cosmologies with machine learning. Mon. Not. R. Astron. Soc. **487**(1), 104–122 (2019). arXiv:1810.11027

40. A. Peel, F. Lalande, J.L. Starck, V. Pettorino, J. Merten, C. Giocoli, M. Meneghetti, M. Baldi, Distinguishing standard and modified gravity cosmologies with machine learning. Phys. Rev. D **100**(2), 023508 (2019). arXiv:1810.11030

41. D. Ribli, B.Á. Pataki, J.M.Z. Matilla, D. Hsu, Z. Haiman, I. Csabai, Weak lensing cosmology with convolutional neural networks on noisy data. Mon. Not. R. Astron. Soc. **490**(2), 1843–1860 (2019). arXiv:1902.03663

42. J. Fluri, T. Kacprzak, A. Lucchi, A. Refregier, A. Amara, T. Hofmann, A. Schneider, Cosmological constraints with deep learning from KiDS-450 weak lensing maps. Phys. Rev. D **100**(6), 063514 (2019). arXiv:1906.03156

43. S. Pan, M. Liu, J. Forero-Romero, C.G. Sabiu, Z. Li, H. Miao, X.D. Li, Cosmological parameter estimation from large-scale structure deep learning. Sci. China Phys. Mech. Astron. **63**(11), 110412 (2020). arXiv:1908.10590

44. M. Ntampaka, D.J. Eisenstein, S. Yuan, L.H. Garrison, A hybrid deep learning approach to cosmological constraints from galaxy redshift surveys. arXiv:1909.10527

45. J.M.Z. Matilla, M. Sharma, D. Hsu, Z. Haiman, Interpreting deep learning models for weak lensing. Phys. Rev. D **102**(12), 123506 (2020). arXiv:2007.06529

46. F. Villaescusa-Navarro, S. Genel, D. Angles-Alcazar, L. Thiele, R. Dave, D. Narayanan, A. Nicola, Y. Li, P. Villanueva-Domingo, B. Wandelt, et al., The CAMELS multifield data set: learning

the universe's fundamental parameters with artificial intelligence. Astrophys. J. Suppl. **259**(2), 61 (2022). arXiv:2109.10915

47. H.M. Kamdar, M.J. Turk, R.J. Brunner, Machine learning and cosmological simulations-I. Semi-analytical models. Mon. Not. R. Astron. Soc. **455**(1), 642–658 (2016). arXiv:1510.06402

48. H.M. Kamdar, M.J. Turk, R.J. Brunner, Machine learning and cosmological simulations-II. Hydrodynamical simulations. Mon. Not. R. Astron. Soc. **457**(2), 1162–1179 (2016). arXiv:1510.07659

49. L. Lucie-Smith, H.V. Peiris, A. Pontzen, M. Lochner, Machine learning cosmological structure formation. Mon. Not. R. Astron. Soc. **479**(3), 3405–3414 (2018). arXiv:1802.04271

50. S. He, Y. Li, Y. Feng, S. Ho, S. Ravanbakhsh, W. Chen, B. Póczos, Learning to predict the cosmological structure formation. Proc. Nat. Acad. Sci. **116**(28), 13825–13832 (2019). arXiv:1811.06533

51. D.K. Ramanah, T. Charnock, G. Lavaux, Painting halos from cosmic density fields of dark matter with physically motivated neural networks. Phys. Rev. D **100**(4), 043515 (2019). arXiv:1903.10524

52. L. Lucie-Smith, H.V. Peiris, A. Pontzen, An interpretable machine learning framework for dark matter halo formation. Mon. Not. R. Astron. Soc. **490**(1), 331–342 (2019). arXiv:1906.06339

53. M. Tsizh, B. Novosyadlyj, Y. Holovatch, N.I. Libeskind, Large-scale structures in the ΛCDM Universe: network analysis and machine learning. Mon. Not. R. Astron. Soc. **495**(1), 1311–1320 (2020). arXiv:1910.07868

54. K. Murakami, A.J. Nishizawa, Identifying cosmological information in a deep neural network. arXiv:2012.03778

55. J. Chacón, J.A. Vázquez, E. Almaraz, Classification algorithms applied to structure formation simulations. Astron. Comput. **38**, 100527 (2022). arXiv:2106.06587

56. R. von Marttens, L. Casarini, N.R. Napolitano, S. Wu, V. Amaro, R. Li, C. Tortora, A. Canabarro, Y. Wang, Inferring galaxy dark halo properties from visible matter with machine learning. Mon. Not. R. Astron. Soc. arXiv:2111.01185

57. D. Piras, B. Joachimi, F. Villaescusa-Navarro, Fast and realistic large-scale structure from machine-learning-augmented random field simulations. arXiv:2205.07898

58. S. Hassan, A. Liu, S. Kohn, P. La Plante, Identifying reionization sources from 21 cm maps using convolutional neural networks. Mon. Not. R. Astron. Soc. **483**(2), 2524–2537 (2019). arXiv:1807.03317

59. N. Gillet, A. Mesinger, B. Greig, A. Liu, G. Ucci, Deep learning from 21-cm tomography of the cosmic dawn and reionization. Mon. Not. R. Astron. Soc. **484**(1), 282–293 (2019). arXiv:1805.02699

60. J. Chardin, G. Uhlrich, D. Aubert, N. Deparis, N. Gillet, P. Ocvirk, J. Lewis, A deep learning model to emulate simulations of cosmic reionization. Mon. Not. R. Astron. Soc. **490**(1), 1055–1065 (2019). arXiv:1905.06958

61. P. La Plante, M. Ntampaka, Machine learning applied to the reionization history of the universe in the 21 cm signal. Astrophys. J. **810**, 110 (2019). arXiv:1810.08211

62. T. Mangena, S. Hassan, M.G. Santos, Constraining the reionization history using deep learning from 21 cm tomography with the square kilometre array. Mon. Not. R. Astron. Soc. **494**(1), 600–606 (2020). arXiv:2003.04905

63. S. Hassan, S. Andrianomena, C. Doughty, Constraining the astrophysics and cosmology from 21 cm tomography using deep learning with the SKA. Mon. Not. R. Astron. Soc. **494**(4), 5761–5774 (2020). arXiv:1907.07787

64. D. Prelogović, A. Mesinger, S. Murray, G. Fiameni, N. Gillet, Machine learning astrophysics from 21 cm lightcones: impact of network architectures and signal contamination. Mon. Not. R. Astron. Soc. **509**(3), 3852–3867 (2021). arXiv:2107.00018

65. A.A. Collister, O. Lahav, ANNz: estimating photometric redshifts using artificial neural networks. Publ. Astron. Soc. Pac. **116**, 345–351 (2004). arXiv:astro-ph/0311058

66. R. Hogan, M. Fairbairn, N. Seeburn, GAz: a genetic algorithm for photometric redshift estimation. Mon. Not. R. Astron. Soc. **449**(2), 2040–2046 (2015). arXiv:1412.5997

67. I. Sadeh, F.B. Abdalla, O. Lahav, ANNz2-photometric redshift and probability distribution function estimation using machine learning. Publ. Astron. Soc. Pac. **128**(968), 104502 (2016). arXiv:1507.00490

68. M. Bilicki, et al., Photometric redshifts for the kilo-degree survey. Machine-learning analysis with artificial neural networks. Astron. Astrophys. **616**, A69 (2018). arXiv:1709.04205

69. Z. Gomes, M.J. Jarvis, I.A. Almosallam, S.J. Roberts, Improving photometric redshift estimation using GPz: size information, post processing and improved photometry. Mon. Not. R. Astron. Soc. **475**(1), 331–342 (2018). arXiv:1712.02256

70. G. Desprez, et al., [Euclid], Euclid preparation: X. The *Euclid* photometric-redshift challenge. Astron. Astrophys. **644**, A31 (2020). arXiv:2009.12112

71. L. Cabayol, M. Eriksen, A. Amara, J. Carretero, R. Casas, F.J. Castander, J. De Vicente, E. Fernández, J. García-Bellido, E. Gaztanaga, et al., The PAU survey: estimating galaxy photometry with deep learning. Mon. Not. R. Astron. Soc. **506**(3), 4048–4069 (2021). arXiv:2104.02778

72. S. Kunsági-Máté, R. Beck, I. Szapudi, I. Csabai, Photometric redshifts for quasars from WISE-PS1-STRM. (2022). arXiv:2206.01440

73. A. Kurcz, M. Bilicki, A. Solarz, M. Krupa, A. Pollo, K. Małek, Towards automatic classification of all WISE sources. Astron. Astrophys. **592**, A25 (2016). arXiv:1604.04229

74. E.J. Kim, R.J. Brunner, Star-galaxy classification using deep convolutional neural networks. Mon. Not. R. Astron. Soc. **464**(4), 4463–4475 (2017). arXiv:1608.04369

75. R. Beck, I. Szapudi, H. Flewelling, C. Holmberg, E. Magnier, PS1-STRM: neural network source classification and photometric redshift catalogue for PS1 3π DR1. Mon. Not. R. Astron. Soc. **500**(2), 1633–1644 (2020). arXiv:1910.10167

76. P.O. Baqui, et al., The miniJPAS survey: star-galaxy classification using machine learning. Astron. Astrophys. **645**, A87 (2021). arXiv:2007.07622

77. M. Lochner, J.D. McEwen, H.V. Peiris, O. Lahav, M.K. Winter, Photometric supernova classification with machine learning. Astrophys. J. Suppl. **225**(2), 31 (2016). arXiv:1603.00882

78. D. Muthukrishna, D. Parkinson, B. Tucker, DASH: deep learning for the automated spectral classification of supernovae and their hosts. Astrophys. J. **885**, 85 (2019). arXiv:1903.02557

79. D. Muthukrishna, G. Narayan, K.S. Mandel, R. Biswas, R. Hložek, RAPID: early classification of explosive transients using deep learning. Publ. Astron. Soc. Pac. **131**(1005), 118002 (2019). arXiv:1904.00014

80. C. Fremling, X.J. Hall, M.W. Coughlin, A.S. Dahiwale, D.A. Duev, M.J. Graham, M.M. Kasliwal, E.C. Kool, A.A. Mahabal, A.A. Miller, et al., SNIascore: deep-learning classification of low-resolution supernova spectra. Astrophys. J. Lett. **917**(1), L2 (2021). arXiv:2104.12980

81. M. Seikel, C. Clarkson, M. Smith, Reconstruction of dark energy and expansion dynamics using Gaussian processes. JCAP **06**, 036 (2012). arXiv:1204.2832. GaPP is available at https://github.com/astrobengaly/GaPP

82. R. Jimenez, L. Verde, T. Treu, D. Stern, Constraints on the equation of state of dark energy and the Hubble constant from stellar ages and the CMB. Astrophys. J. **593**, 622–629 (2003). arXiv:astro-ph/0302560

83. J. Simon, L. Verde, R. Jimenez, Constraints on the redshift dependence of the dark energy potential. Phys. Rev. D **71**, 123001 (2005). arXiv:astro-ph/0412269

84. D. Stern, R. Jimenez, L. Verde, M. Kamionkowski, S.A. Stanford, Cosmic chronometers: constraining the equation of state

of dark energy. I: H(z) Measurements. JCAP **02**, 008 (2010). arXiv:0907.3149

85. M. Moresco, A. Cimatti, R. Jimenez, L. Pozzetti, G. Zamorani, M. Bolzonella, J. Dunlop, F. Lamareille, M. Mignoli, H. Pearce, et al., Improved constraints on the expansion rate of the Universe up to z 1.1 from the spectroscopic evolution of cosmic chronometers. JCAP **08**, 006 (2012). arXiv:1201.3609

86. C. Zhang, H. Zhang, S. Yuan, S. Liu, T.-J. Zhang, Y.-C. Sun, Four new observational $H(z)$ data from luminous red galaxies of Sloan digital sky survey data release seven. Res. Astron. Astrophys. **14**, 1221–1233 (2014). arXiv:1207.4541

87. M. Moresco, Raising the bar: new constraints on the Hubble parameter with cosmic chronometers at z ∼ 2. Mon. Not. R. Astron. Soc. **450**(1), L16–L20 (2015). arXiv:1503.01116

88. M. Moresco, L. Pozzetti, A. Cimatti, R. Jimenez, C. Maraston, L. Verde, D. Thomas, A. Citro, R. Tojeiro, D. Wilkinson, A 6% measurement of the Hubble parameter at $z \sim 0.45$: direct evidence of the epoch of cosmic re-acceleration. JCAP **05**, 014 (2016). arXiv:1601.01701

89. A.L. Ratsimbazafy, S.I. Loubser, S.M. Crawford, C.M. Cress, B.A. Bassett, R.C. Nichol, P. Väisänen, Age-dating luminous red galaxies observed with the Southern African large telescope. Mon. Not. R. Astron. Soc. **467**(3), 3239–3254 (2017). arXiv:1702.00418

90. F. Pedregosa et al., Scikit-learn: machine learning in Python. J. Mach. Learn. Res. **12**, 2825 (2011). https://scikit-learn.org/stable/index.html

91. L. Breiman, J. Friedman, R. Olshen, C. Stone, *Classification and Regression Trees* (Wadsworth, Belmont, 1984)

92. D.E. Rumelhart, G.E. Hinton, R.J. Williams, Learning representations by back-propagating errors. Nature **323**, 533 (1986)

93. J.H. Friedman, Greedy function approximation: a gradient boosting machine. Ann. Stat. **29**, 1189

94. C.M. Bishop, *Pattern Recognition and Machine Learning* (Springer, Berlin, 2006)

95. A.J. Smola, B. Schölkopf, A tutorial on support vector regression. Stat. Comput. **14**, 199 (2004)